IEEE Access
Multidisciplinary | Rapid Review | Open Access Journal

Received March 23, 2021, accepted March 28, 2021, date of publication April 14, 2021, date of current version April 27, 2021.

Digital Object Identifier 10.1109/ACCESS.2021.3073246

Time Reverse Equalization Algorithm for 16 QAM Coherent Optical Communication Systems

JUNXIONG ZHANG, WEIMIN WU, AND XIAOHU GE, (Senior Member, IEEE)
School of Electronic Information and Communications, Huazhong University of Science and Technology, Wuhan 430074, China

Corresponding author: Weimin Wu (wuwm@hust.edu.cn)

This work was supported by the National Key Research and Development Program of China under Grant 2020YFB1806605.

ABSTRACT The high speed rotation of state of polarization (RSOP) is a key issue for 16 quadrature amplitude modulation (QAM) coherent optical polarization division multiplexing (PDM) communication systems in strong lightning weather. To reduce the bit error rate (BER) caused by the high speed of RSOP, the historical information is first proposed to correct the demodulation process in coherent optical communication systems. By adding the time reverse error term into the cost function, a new equalization algorithm is proposed for coherent optical communication systems. Compared with the conventional Multi-modulus Algorithm (MMA), simulation results show that the average BER and steady-state error (SSE) of the new algorithm is reduced by 33.47% and 4.08%, respectively. Moreover, the average tolerance of RSOP of the new algorithm is increased by 28.57% compared with the MMA in 16 QAM coherent optical PDM communication systems.

INDEX TERMS Coherent optical PDM, time reverse error, 16 QAM, RSOP, SSE, BER.

I. INTRODUCTION

In modern communication networks, to improve the spectrum efficiency always is an key issue [1]. The polarization division multiplexing (PDM) technology is widely used to improve the spectrum efficiency of coherent optical communication systems [2]–[6]. Based on the polarization characteristics of light, the PDM technology uses two orthogonal optical carrier polarization states to simultaneously propagate two signals, which can double the capacity of communication systems [7]. However, some factors such as mechanical vibration and extreme weather may lead to rapid changes of signal polarization state in a coherent optical communication system [8]. This type of signal effect is called the rotation of state of polarization (RSOP). The fastest speed of RSOP caused by mechanical disturbance is 45,000 rotations per second [9], but thunderstorms can cause severe interference to the RSOP of coherent optical communication systems. Under the influence of strong lightning strikes, the speed of RSOP can reach the level of 10^6 rad/s (Mrad/s) [10]. The high-speed RSOP will obviously increase the bit error rate (BER) of coherent optical communication systems [11]. Therefore, it is a great challenge to design a new equalization algorithm to overcome issues caused by the high-speed RSOP in coherent optical communication systems.

According to whether a training sequence is required, equalization algorithms can be divided into non-blind equalization algorithms and blind equalization algorithms [12]. In the non-blind equalization algorithm, the training sequence is embedded in the transmission sequence and transmitted in the channel together. The specific information of the training sequence is known in advance at the receiver, so the receiver can evaluate the channel loss and adjust the equalizer coefficients by calculating the error between the received training sequence and the transmitted training sequence. The disadvantage of non-blind equalization algorithms is the reduction of spectral efficiency. Especially under the influence of strong lightning, the channel changes at a high speed and the spectrum efficiency of non-blind equalization algorithms will be further reduced. However, blind equalization algorithms or adaptive equalization algorithms do not require a training sequence and can adjust the equalizer coefficients adaptively [13]. Compared with non-blind equalization algorithms, blind equalization algorithms are more suitable for high-speed real-time transmission systems and has higher spectrum utilization. Hence, to improve spectrum efficiency, adaptive equalization algorithms are developed for the equalization of RSOP in coherent optical communication systems.

The associate editor coordinating the review of this manuscript and approving it for publication was Joewono Widjaja.

The constant modulus algorithm (CMA) is a classic adaptive equalization algorithm [14]. CMA uses the steepest descent method to minimize the cost function of the algorithm, which is composed of error between the actual output signals and ideal output signals. In 2007, the CMA was applied to quadrature phase shift keying (QPSK) coherent optical PDM systems [15]. However, the CMA has a slow convergence speed and does not consider the influence of the channel on phases of the transmitted signals. Given problems of the CMA, Yu *et al.* [16] proposed to use the Stokes space (SS) to improve the convergence speed of CMA in coherent optical communication systems. Bosco *et al.* [17] proposed to convert the cost function of CMA into the SS for calculation, which improves the tolerance of signal-to-noise ratio (SNR) in coherent optical communication systems. Another adaptive equalization algorithm different from CMA is an SS-based equalization algorithm [18]–[20]. The SS-based equalization algorithm directly converts received signals into the SS and obtains a plane composed of received signals. The RSOP can be calculated by analyzing the geometric information of the normal vector of the plane composed of received signals. Compared with the CMA, the SS-based equalization algorithm has a faster convergence speed. Based on the SS, R. Borkowski proposed an identification algorithm for the modulation format of coherent optical signals. The recognized modulation format can be used as an additional information for improving the performance of equalization algorithms [21]. N. J. Muga and A. N. Pinto proposed a new method to further improve the tolerance of channel loss of SS-based equalization algorithms [22]. However, the disadvantage of the SS-based algorithm is that the fitting plane requires a large number of received signals to get an accurate plane, which means that the channel needs to be static or change very slowly. Hence, the SS-based algorithm is not suitable for high-speed RSOP situations. To overcome the disadvantage of the SS-based algorithm, N. J. Muga and A. N. Pinto proposed an adaptive SS-based equalization algorithm, which can deal with the QPSK signals in high-speed RSOP situations [23]. But the adaptive SS-based equalization algorithm is not suitable for the 16 quadrature amplitude modulation (QAM) signals in high-speed RSOP situations. The QPSK signals constitutes only one plane in the SS, while the 16 QAM signals constitutes five planes in the SS. The calculation of normal vectors of five planes requires a very large number of received signals. When the signal modulation format is 16 QAM and the RSOP speed is high, the existing algorithm cannot calculate the channel loss in real time. Besides, when the CMA was applied to QAM format signals, the BER of coherent optical communication systems is greatly increased and cannot satisfy the quality of service (QoS) of coherent optical communication systems [24].

To satisfy the QoS of QAM format signals in coherent optical communication systems, the multi-modulus algorithm (MMA) was proposed to divide the output of equalizer into a real part and an imaginary part [25], which are equalized separately to offset the phase loss. However, the MMA cannot reduce the BER of equalization process under high-speed RSOP in coherent optical communication systems.

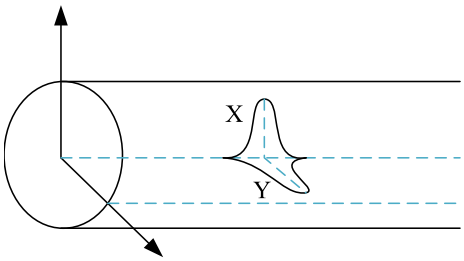

FIGURE 1. Schematic diagram of coherent optical PDM transmissions.

Consider a 16 QAM coherent optical PDM system, we have proposed a new equalization algorithm based on the time reverse error to solve the high BER problem of coherent optical communication systems with high-speed RSOP. The contributions of this paper are summarized as follows:

1) Based on the analysis of the hysteresis effect on the equalization matrix in coherent optical communication systems, the time reverse error idea is first proposed to correct the BER of equalization processes in this paper.
2) Based on the hysteresis effect of the equalization matrix, a new equalization algorithm based on the time reverse error is developed to reduce the BER and steady-state error (SSE). Different with conventional equalization algorithms, the historical information is added into the cost function of the new equalization algorithm for fasting the convergence speed of output signal errors.
3) Simulation results show that the BER and SSE of the new algorithm decrease with the increase of the number of time reverse error terms. Compared with the MMA, the average BER and SSE of the new algorithm is reduced by 33.47% and 4.08%, respectively. Moreover, the average tolerance of RSOP of the new algorithm is increased by 28.57% compared with the MMA.

This paper is organized as follows. The system model is described in Section II. The analysis of the hysteresis effect of the equalization matrix and the explanation of the new algorithm are presented in Section III. The simulation results are illustrated in Section IV. In the end, conclusions are drawn in Section V.

II. SYSTEM MODEL

Figure 1 shows the schematic of coherent optical PDM transmissions, where X is the X-Polarization (X-Pol) signal, Y is the Y-Polarization (Y-Pol) signal. The two signals, i.e., X-Pol and Y-Pol signals are transmitted orthogonally in an optical fiber.

The optical signals suffer many kinds of channel loss such as chromatic dispersion (CD), polarization mode dispersion (PMD) and RSOP during transmission. Hence, the transmission signals need to be equalized at the receiver of coherent optical PDM systems. A typical digital signal processing (DSP) module of the receiver of coherent

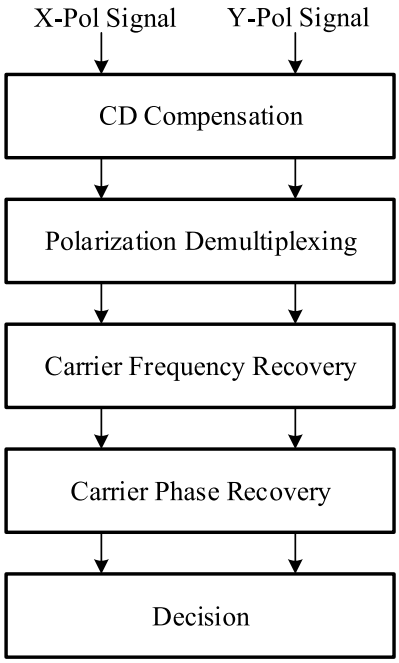

FIGURE 2. Block diagram of coherent optical PDM system.

optical PDM systems is shown in Figure 2 [26]. X-Pol signal and Y-Pol signal need to go through four equalization processes of CD compensation, depolarization multiplexing, carrier frequency recovery and carrier phase recovery. Finally, the equalized X-Pol signal and Y-Pol signal are restored to symbols through the decision circuit. This paper focuses on the equalization algorithm for RSOP and there are many corresponding algorithms for CD and PMD compensation [27]–[29]. Hence, this paper assume other impairments are already compensated in previous parts and only considers three channel impairments in the algorithm, which are carrier frequency offset (CFO), carrier phase noise (CPO), RSOP and additive white Gaussian noise (AWGN).

The input signals of the channel $\mathrm{X}(n)$, $\mathrm{Y}(n)$ and the input signal matrix of the channel $\mathbf{E}(n)$ are given as [30]

$$\mathbf{E}(n) = \begin{bmatrix} \mathrm{X}(n) \\ \mathrm{Y}(n) \end{bmatrix} = \begin{bmatrix} \mathrm{A_X}(n)e^{\mathrm{j}\theta_\mathrm{X}(n)} \\ \mathrm{A_Y}(n)e^{\mathrm{j}\theta_\mathrm{Y}(n)} \end{bmatrix}, \tag{1}$$

where n denotes time value ($n \geq 1$), e denotes the natural constant, j denotes the imaginary unit, $\mathrm{A_X}(n)$ and $\theta_\mathrm{X}(n)$ denote the amplitude and phase of $\mathrm{X}(n)$, $\mathrm{A_Y}(n)$ and $\theta_\mathrm{Y}(n)$ denote the amplitude and phase of $\mathrm{Y}(n)$, respectively.

The mathematical model of time-varying RSOP $\mathbf{R}(n)$ is given as [11]

$$\mathbf{R}(n) = \begin{bmatrix} e^{\mathrm{j}\epsilon}cos\gamma & -e^{\mathrm{j}\sigma}sin\gamma \\ e^{-\mathrm{j}\sigma}sin\gamma & e^{-\mathrm{j}\epsilon}cos\gamma \end{bmatrix}, \tag{2}$$

$$\gamma = \frac{n\omega}{f_s}, \tag{3}$$

where ϵ and σ denote the phase angles, γ denotes the amplitude ratio angle, ω denotes the speed of RSOP, f_s denotes the symbol transmission rate.

The mathematical model of CFO $\mathrm{F}(n)$ is given as [31]

$$\mathrm{F}(n) = e^{\mathrm{j}2\pi f_c \frac{n}{f_s}}, \tag{4}$$

where f_c denotes the value of CFO.

The CPO $\varphi(n)$ is modeled as a Wiener process [32]. The first difference of $\varphi(n)$ is an independent and identically distributed Gaussian random variable with a mean of 0 and a variance of $\frac{2\pi v}{f_s}$, i.e.,

$$[\varphi(n+1) - \varphi(n)\,] \sim N(0, \frac{2\pi v}{f_s}), \tag{5}$$

where v denotes the laser linewidth.

The input signals of the equalizer $\mathrm{Xin}(n)$, $\mathrm{Yin}(n)$ and the input signal matrix of the equalizer $\mathbf{Sig\_in}(n)$ is expressed by [31]

$$\mathbf{Sig\_in}(n) = \begin{bmatrix} \mathrm{Xin}(n) \\ \mathrm{Yin}(n) \end{bmatrix} = \mathbf{R}(n) \cdot \mathbf{E}(n) \cdot \mathrm{F}(n) \cdot e^{\mathrm{j}\varphi(n)} + \mathbf{G}, \tag{6}$$

where $\mathbf{G}$ denotes the matrix of AWGN.

The equalization matrix $\mathbf{H}(n)$ is the inverse of $\mathbf{R}(n)$ [11], i.e.,

$$\mathbf{H}(n) = \begin{bmatrix} e^{-\mathrm{j}\epsilon_s}cos\gamma_s & e^{\mathrm{j}\sigma_s}sin\gamma_s \\ -e^{-\mathrm{j}\sigma_s}sin\gamma_s & e^{\mathrm{j}\epsilon_s}cos\gamma_s \end{bmatrix}, \tag{7}$$

where ϵ_s, σ_s and γ_s denote the estimated value of ϵ, σ and γ respectively.

The output signals of the equalizer $\mathrm{Xout}(n)$, $\mathrm{Yout}(n)$ and the output signal matrix of the equalizer $\mathbf{Sig\_out}(n)$ is expressed by

$$\mathbf{Sig\_out}(n) = \begin{bmatrix} \mathrm{Xout}(n) \\ \mathrm{Yout}(n) \end{bmatrix} = \mathbf{H}(n) \cdot \mathbf{Sig\_in}(n). \tag{8}$$

This paper focuses on the RSOP equalization algorithm, the equalization of CFO and CPO is not included. Hence, in the later analysis of BER, the final output signals $\mathbf{Sig\_fin}(n)$ is used to analyze the BER. $\mathbf{Sig\_fin}(n)$ is given by

$$\mathbf{Sig\_fin}(n) = \mathbf{Sig\_out}(n) \cdot e^{-\mathrm{j}(2\pi f_c \frac{n}{f_s} + \varphi(n))}. \tag{9}$$

III. EQUALIZATION ALGORITHM BASED ON TIME REVERSE ERROR

A. PROBLEM FORMULATION

The principle of the MMA is to minimize the cost function based on actual output signals and ideal output signals in coherent optical PDM systems. In a 16QAM coherent optical PDM system, CFO leads to the rotation of the received constellation with time [26]. Therefore, the ideal output signals obtained in the polarization demultiplexing part is three rings with radii of $\sqrt{2}$, $\sqrt{10}$ and $3\sqrt{2}$ respectively. The ideal output

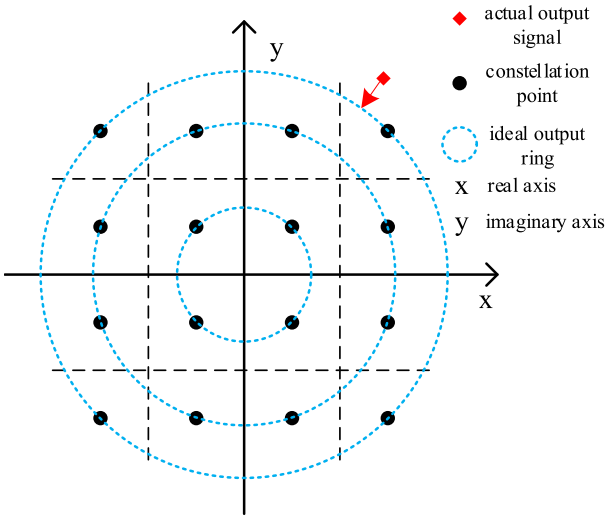

FIGURE 3. 16 QAM-MMA decisions.

signal decision rule is given by [33]

$$\begin{cases} \mathrm{Xideal_r}(n) = \mathrm{Xout_r}(n)\sqrt{2}{R_\mathrm{X}}^{-1}, \\ \mathrm{Xideal_i}(n) = \mathrm{Xout_i}(n)\sqrt{2}{R_\mathrm{X}}^{-1}, \\ R_\mathrm{X} < R_1, \end{cases} \tag{10a}$$

$$\begin{cases} \mathrm{Xideal_r}(n) = \mathrm{Xout_r}(n)\sqrt{10}{R_\mathrm{X}}^{-1}, \\ \mathrm{Xideal_i}(n) = \mathrm{Xout_i}(n)\sqrt{10}{R_\mathrm{X}}^{-1}, \\ R_1 \le R_\mathrm{X} \le R_2, \end{cases} \tag{10b}$$

$$\begin{cases} \mathrm{Xideal_r}(n) = \mathrm{Xout_r}(n)3\sqrt{2}{R_\mathrm{X}}^{-1}, \\ \mathrm{Xideal_i}(n) = \mathrm{Xout_i}(n)3\sqrt{2}{R_\mathrm{X}}^{-1}, \\ R_\mathrm{X} > R_2, \end{cases} \tag{10c}$$

$$\begin{cases} \mathrm{Yideal_r}(n) = \mathrm{Yout_r}(n)\sqrt{2}{R_\mathrm{Y}}^{-1}, \\ \mathrm{Yideal_i}(n) = \mathrm{Yout_i}(n)\sqrt{2}{R_\mathrm{Y}}^{-1}, \\ R_\mathrm{Y} < R_1, \end{cases} \tag{11a}$$

$$\begin{cases} \mathrm{Yideal_r}(n) = \mathrm{Yout_r}(n)\sqrt{10}{R_\mathrm{Y}}^{-1}, \\ \mathrm{Yideal_i}(n) = \mathrm{Yout_i}(n)\sqrt{10}{R_\mathrm{Y}}^{-1}, \\ R_1 \le R_\mathrm{Y} \le R_2, \end{cases} \tag{11b}$$

$$\begin{cases} \mathrm{Yideal_r}(n) = \mathrm{Yout_r}(n)3\sqrt{2}{R_\mathrm{Y}}^{-1}, \\ \mathrm{Yideal_i}(n) = \mathrm{Yout_i}(n)3\sqrt{2}{R_\mathrm{Y}}^{-1}, \\ R_\mathrm{Y} > R_2, \end{cases} \tag{10c}$$

where $R_1 = \frac{2\mathrm{SNR}^{-1}\ln 2 - 8}{2(\sqrt{2}-\sqrt{10})}$, $R_2 = \frac{2\mathrm{SNR}^{-1}\ln 2 + 8}{2(3\sqrt{2}-\sqrt{10})}$, $\mathrm{Xout_r}(n)$ and $\mathrm{Xout_i}(n)$ denote the real and imaginary parts of the actual output signal over the X-Pol signal, $\mathrm{Xideal_r}(n)$ and $\mathrm{Xideal_i}(n)$ denote the real and imaginary parts of the ideal output over the X-Pol signal, $\mathrm{Yout_r}(n)$ and $\mathrm{Yout_i}(n)$ denote the real and imaginary parts of the actual output over the Y-Pol signal, $\mathrm{Yideal_r}(n)$ and $\mathrm{Yideal_i}(n)$denote the real and imaginary parts of the ideal output over the Y-Pol signal, R_X denotes the modulus of $\mathrm{Xout}(n)$, R_Y denotes the modulus of $\mathrm{Yout}(n)$ and $\ln(\cdot)$ denotes the logarithmic function with base e. The 16 QAM-MMA decisions is shown in Figure 3.

The total cost function of the MMA $\mathrm{J}(n)$ is given as [34]

$$\mathrm{J}(n) = \mathrm{J_X}(n) + \mathrm{J_Y}(n), \tag{12a}$$

$$\mathrm{J_X}(n) = \mathrm{E}\left\{\mathrm{q}(n)^2 + \mathrm{p}(n)^2\right\}, \tag{12b}$$

$$\mathrm{J_Y}(n) = \mathrm{E}\left\{\mathrm{z}(n)^2 + \mathrm{m}(n)^2\right\}, \tag{12c}$$

$$\mathrm{q}(n) = \mathrm{Xout_r}(n)^2 - \frac{\mathrm{E}\left\{\mathrm{Xideal_r}(n)^4\right\}}{\mathrm{E}\left\{\mathrm{Xideal_r}(n)^2\right\}}, \tag{12d}$$

$$\mathrm{p}(n) = \mathrm{Xout_i}(n)^2 - \frac{\mathrm{E}\left\{\mathrm{Xideal_i}(n)^4\right\}}{\mathrm{E}\left\{\mathrm{Xideal_i}(n)^2\right\}}, \tag{12e}$$

$$\mathrm{z}(n) = \mathrm{Yout_r}(n)^2 - \frac{\mathrm{E}\left\{\mathrm{Yideal_r}(n)^4\right\}}{\mathrm{E}\left\{\mathrm{Yideal_r}(n)^2\right\}}, \tag{12f}$$

$$\mathrm{m}(n) = \mathrm{Yout_i}(n)^2 - \frac{\mathrm{E}\left\{\mathrm{Yideal_i}(n)^4\right\}}{\mathrm{E}\left\{\mathrm{Yideal_i}(n)^2\right\}}, \tag{12g}$$

where $\mathrm{J_X}(n)$ denotes the cost function of the X-Pol signal, $\mathrm{J_Y}(n)$ denotes the cost function of the Y-Pol signal, $\mathrm{E}\{\cdot\}$ denotes the expectation operation.

According to the idea of the steepest descent [35], the expected value can be replaced by the instantaneous value and the equalization matrix coefficients are updated according to the gradient of $\mathrm{J}(n)$. Furthermore, consider the influence of CFO, the cost function of MMA should be corrected by using probability weights $\mathrm{D_{0X}}(n)$ and $\mathrm{D_{0Y}}(n)$ [36]. Hence, the final cost function $\mathrm{J_0}(n)$ is given as

$$\mathrm{J_0}(n) = \mathrm{J_{0X}}(n) + \mathrm{J_{0Y}}(n), \tag{13a}$$

$$\begin{cases} \mathrm{J_{0X}}(n) = \mathrm{D_{0X}}(n)\left[\mathrm{q_0}(n)^2 + \mathrm{p_0}(n)^2\right], \\ \mathrm{D_{0X}}(n) = 0.75, \quad R_\mathrm{X} < R_1, \\ \mathrm{D_{0X}}(n) = 1.5, \quad R_1 \le R_\mathrm{X} \le R_2, \\ \mathrm{D_{0X}}(n) = 0.75, \quad R_\mathrm{X} > R_2, \end{cases} \tag{13b}$$

$$\begin{cases} \mathrm{J_{0Y}}(n) = \mathrm{D_{0Y}}(n)\left[\mathrm{z_0}(n)^2 + \mathrm{m_0}(n)^2\right], \\ \mathrm{D_{0Y}}(n) = 0.75, \quad R_\mathrm{Y} < R_1, \\ \mathrm{D_{0Y}}(n) = 1.5, \quad R_1 \le R_\mathrm{Y} \le R_2, \\ \mathrm{D_{0Y}}(n) = 0.75, \quad R_\mathrm{Y} > R_2. \end{cases} \tag{13c}$$

$$\mathrm{q_0}(n) = \mathrm{Xout_r}(n)^2 - \mathrm{Xideal_r}(n)^2, \tag{13d}$$

$$\mathrm{p_0}(n) = \mathrm{Xout_i}(n)^2 - \mathrm{Xideal_i}(n)^2, \tag{13e}$$

$$\mathrm{z_0}(n) = \mathrm{Yout_r}(n)^2 - \mathrm{Yideal_r}(n)^2, \tag{13f}$$

$$\mathrm{m_0}(n) = \mathrm{Yout_i}(n)^2 - \mathrm{Yideal_i}(n)^2. \tag{13g}$$

The update formula of equalization matrix coefficients is given as

$$\begin{bmatrix} \gamma_s(n+1) \\ \epsilon_s(n+1) \\ \sigma_s(n+1) \end{bmatrix} = \begin{bmatrix} \gamma_s(n) \\ \epsilon_s(n) \\ \sigma_s(n) \end{bmatrix} + \begin{bmatrix} \mu_1 \dfrac{\partial \mathrm{J_0}(n)}{\partial \gamma_s(n)} \\ \mu_2 \dfrac{\partial \mathrm{J_0}(n)}{\partial \epsilon_s(n)} \\ \mu_3 \dfrac{\partial \mathrm{J_0}(n)}{\partial \sigma_s(n)} \end{bmatrix}, \tag{14a}$$

$$\begin{bmatrix} \frac{\partial J_{0X}(n)}{\partial \gamma_s(n)} \\ \frac{\partial J_{0X}(n)}{\partial \epsilon_s(n)} \\ \frac{\partial J_{0X}(n)}{\partial \sigma_s(n)} \end{bmatrix} = \mathbf{V}_{0X}(n) + \mathbf{T}_{0X}(n), \tag{14b}$$

$$\mathbf{V}_{0X}(n) = \begin{bmatrix} Q_0(n)\mathrm{Re}\{W_0(n)\} \\ Q_0(n)\mathrm{Im}\{L_0(n)\}\, cos\gamma_s(n) \\ Q_0(n)\mathrm{Im}\{-K_0(n)\}\, sin\gamma_s(n) \end{bmatrix}, \tag{14c}$$

$$\mathbf{T}_{0X}(n) = \begin{bmatrix} P_0(n)\mathrm{Im}\{W_0(n)\} \\ P_0(n)\mathrm{Re}\{-L_0(n)\}\, cos\gamma_s(n) \\ P_0(n)\mathrm{Re}\{K_0(n)\}\, sin\gamma_s(n) \end{bmatrix}, \tag{14d}$$

$$\begin{bmatrix} \frac{\partial J_{0Y}(n)}{\partial \gamma_s(n)} \\ \frac{\partial J_{0Y}(n)}{\partial \epsilon_s(n)} \\ \frac{\partial J_{0Y}(n)}{\partial \sigma_s(n)} \end{bmatrix} = \mathbf{V}_{0Y}(n) + \mathbf{T}_{0Y}(n), \tag{14e}$$

$$\mathbf{V}_{0Y}(n) = \begin{bmatrix} Z_0(n)\mathrm{Re}\{W_0(n)\} \\ Z_0(n)\mathrm{Im}\{L_0(n)\}\, cos\gamma_s(n) \\ Z_0(n)\mathrm{Im}\{-K_0(n)\}\, sin\gamma_s(n) \end{bmatrix}, \tag{14f}$$

$$\mathbf{T}_{0Y}(n) = \begin{bmatrix} M_0(n)\mathrm{Im}\{W_0(n)\} \\ M_0(n)\mathrm{Re}\{-L_0(n)\}\, cos\gamma_s(n) \\ M_0(n)\mathrm{Re}\{K_0(n)\}\, sin\gamma_s(n) \end{bmatrix}, \tag{14g}$$

$$L_0(n) = e^{-j\epsilon_s(n)}\mathrm{Xin}(n), \tag{14h}$$

$$K_0(n) = -e^{-j\sigma_s(n)}\mathrm{Yin}(n), \tag{14i}$$

$$W_0(n) = -L_0(n) sin\gamma_s(n) + K_0(n) cos\gamma_s(n), \tag{14j}$$

$$Q_0(n) = \mathrm{Xout_r}(n) q_0(n), \tag{14k}$$

$$P_0(n) = \mathrm{Xout_i}(n) p_0(n), \tag{14l}$$

$$Z_0(n) = \mathrm{Yout_r}(n) z_0(n), \tag{14m}$$

$$M_0(n) = \mathrm{Yout_i}(n) m_0(n), \tag{14n}$$

where μ_1, μ_2 and μ_3 denotes the step size, Re $\{\cdot\}$ denotes the operation to extract the real part, Im $\{\cdot\}$ denotes the operation to extract the imaginary part and ∂ denotes seeking partial derivative.

The MMA solves problems of the CMA and can improve the quality of equalization of QAM format signals. However, the MMA still has problems: the cost function only contains the difference between the actual output signal and the ideal output signal at the current moment, which means the MMA only considers the current input and ignores the historical input.

In this paper, $\mathbf{H}(n)$ is used to equalize $\mathbf{Sig\_in}(n-k)$, $(k = 0, 1, 2, \ldots)$, for getting the output signal $\mathbf{Sig\_out}_k(n-k)$, i.e., $\mathbf{Sig\_out}_k(n-k) = \mathbf{H}(n) \cdot \mathbf{Sig\_in}(n-k)$. The output signal sequence is written as $\mathbf{Sig\_out}_k$ and the output signal error sequence is written as $\mathbf{J}_k$. This equalization process is called the time reverse equalization with tracing back to the time $n-k$. when $k = 0$, the equalization process is the regular equalization, i.e., $\mathbf{Sig\_out}_0(n) = \mathbf{H}(n) \cdot \mathbf{Sig\_in}(n)$ and the output signal sequence is written as $\mathbf{Sig\_out}_0$. Figure 4(a) illustrates a general time reverse equalization process and Figure 4(b) illustrates the time reverse equalization with tracing back to the time $n-1$, i.e., $k = 1$.

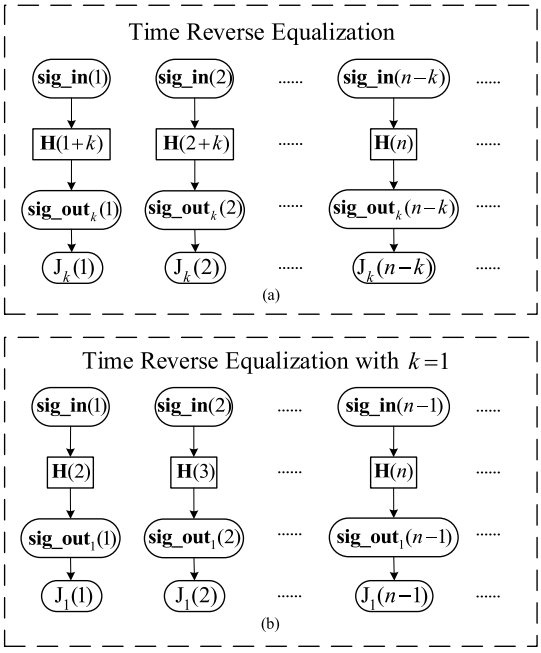

FIGURE 4. Schematic diagram of time reverse equalization.

Figure 5 shows the lg(BER) of $\mathbf{Sig\_out}_k$ with different RSOPs and different k values in 16 QAM coherent optical PDM systems, where lg$(\cdot)$ is the logarithmic function with base 10. Without loss of generality, parameters of simulation in Figure 5 are configured as: SNR is 20 dB, the number of symbols N is 2^{18}, f_s is 28 Gbaud/s, f_c is 1GHz, v is 1MHz, μ_1, μ_2 and μ_3 are 5×10^{-4}, 1.6×10^{-6} and 1.5×10^{-5}, respectively. RSOP starts from 50 Mrad/s, performs 50 simulations every 40 Mrad/s and calculates the average BER.

The simulation results in Figure 5 illustrate that there exists a minimal value for the lg(BER) corresponding to the $k_{\min}$ under each RSOP configuration. The minimal lg(BER) values of Figure 5(a), (b), (c) and (d) are -4.1065, -4.0001, -3.7345 and -3.1823, corresponding to the 19, 19, 20 and 22, respectively. Based on results of Figure 5(a)-(d), the lg(BER) of $\mathbf{Sig\_out}_k$ decreases when k is increased from 0 to $k_{\min}$, i.e., the lg(BER) of $\mathbf{Sig\_out}_{k_{\min}}$ < the lg(BER) of $\mathbf{Sig\_out}_{k_{\min-1}}$ < the lg(BER) of $\mathbf{Sig\_out}_{k_{\min-2}}$ < ... < the lg(BER) of $\mathbf{Sig\_out}_1$ < the lg(BER) of $\mathbf{Sig\_out}_0$. Besides, the lower the lg(BER) of $\mathbf{Sig\_out}_k$ with the lower the $\mathbf{J}_k$. So the following results is obtained: $\mathbf{J}_{k_{\min}} < \mathbf{J}_{k_{\min-1}} < \ldots < \mathbf{J}_0$. Moreover, it can be seen that the $\mathbf{J}_k$ of $\mathbf{Sig\_out}_k$ is determined by the equalization effect of matrixes from $\mathbf{Sig\_out}_k(n-k) = \mathbf{H}(n) \cdot \mathbf{Sig\_in}(n-k)$, i.e, the better the equalization effect of matrixes with the lower the $\mathbf{J}_k$ of $\mathbf{Sig\_out}_k$. Hence, it can be seen that for every $\mathbf{Sig\_in}(n)$, $(n = 1, 2, \ldots)$, the following results is obtained: the equalization effect of $\mathbf{H}(n + k_{\min})$ > the equalization effect of $\mathbf{H}(n + k_{\min-1})$ > ... > the equalization effect of $\mathbf{H}(n+1)$ > the equalization effect of $\mathbf{H}(n)$.

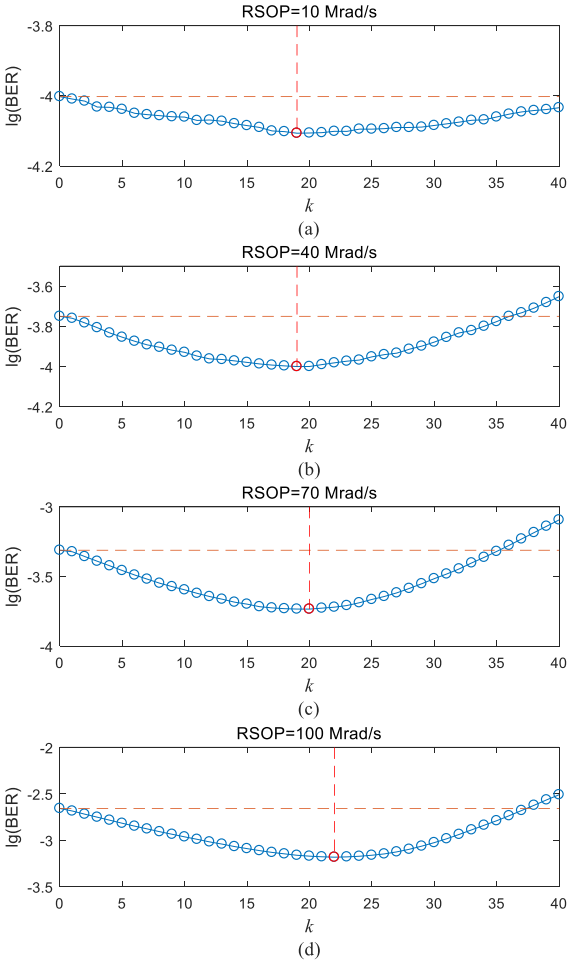

FIGURE 5. lg(BER) of the time reverse equalization.

When the input signal of the equalizer in (6) is a non-stationary signal, the cost function i.e., (13a) appears as a time-varying concave surface in geometric space [35]. The stationary point of the cost function is continuously moving and the equalization matrix cannot accurately track the stationary point at all times. Hence, the equalization matrix can only be close to the stagnation point and always lags behind the stagnation point. In this paper, this result is referred as to the hysteresis effect of equalization matrix.

Due to the real-time requirement of coherent optical communication systems, the time reverse equalization idea cannot be directly used in existing systems to cover historical output signals, i.e, the output signal sequence must be $\mathbf{Sig\_out}_0$. Based on (8), the BER of $\mathbf{Sig\_out}_0$ can be reduced by improving the equalization effect of $\mathbf{H}(n)$. For every $\mathbf{Sig\_in}(n)$, the equalization effect of $\mathbf{H}(n)$ can be improved by adding the time reverse error $\mathrm{J}_k(n-k)$ into the cost function (13a). $\mathrm{J}_1(n-1)$ is added to (13a), the new cost function J_{new} and the new equalization matrix coefficients update formula are given as

$$\mathrm{J}_{new}(n) = \mathrm{J}_0(n) + \mathrm{J}_1(n-1), \tag{15a}$$

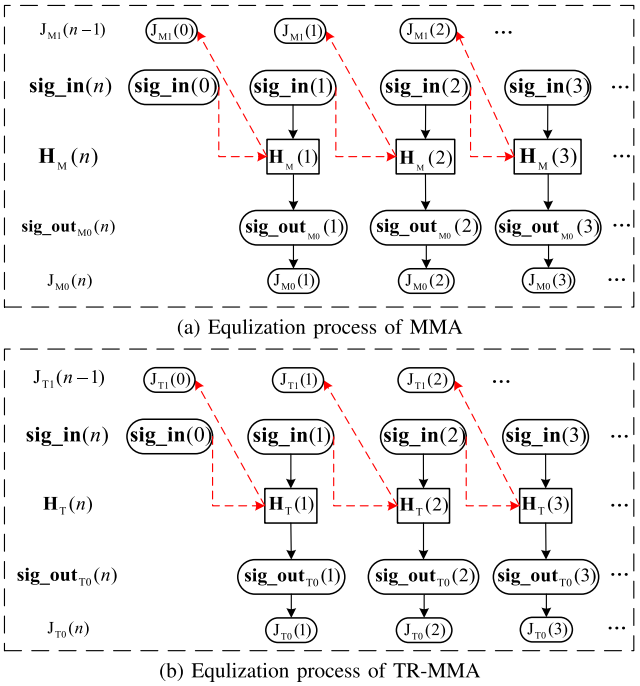

FIGURE 6. Equalization process diagram of MMA and TR-MMA.

$$\begin{bmatrix} \gamma_s(n+1) \\ \epsilon_s(n+1) \\ \sigma_s(n+1) \end{bmatrix} = \begin{bmatrix} \gamma_s(n) \\ \epsilon_s(n) \\ \sigma_s(n) \end{bmatrix} + \begin{bmatrix} \mu_4 \dfrac{\partial \mathrm{J}_{new}(n)}{\partial \gamma_s(n)} \\ \mu_5 \dfrac{\partial \mathrm{J}_{new}(n)}{\partial \epsilon_s(n)} \\ \mu_6 \dfrac{\partial \mathrm{J}_{new}(n)}{\partial \sigma_s(n)} \end{bmatrix}, \tag{15b}$$

where μ_4, μ_5 and μ_6 are the step sizes of new algorithm.

Based on (15), a new algorithm, i.e., Time Reverse MMA (TR-MMA) is proposed to improve the performance of MMA in 16 QAM coherent optical PDM systems. The equalization process of MMA and TR-MMA is illustrated in Figure 6. In Figure 6(a), $\mathrm{J}_{\mathrm{M1}}(n-1)$ is the $\mathrm{J}_1(n-1)$ of the MMA, $\mathrm{J}_{\mathrm{M0}}(n)$ is the $\mathrm{J}_0(n)$ of the MMA, $\mathbf{H}_{\mathrm{M}}(n)$ is the $\mathbf{H}(n)$ of the MMA. In Figure 6(b), $\mathrm{J}_{\mathrm{T1}}(n-1)$ is the $\mathrm{J}_1(n-1)$ of the TR-MMA, $\mathrm{J}_{\mathrm{T0}}(n)$ is the $\mathrm{J}_0(n)$ of the TR-MMA, $\mathbf{H}_{\mathrm{T}}(n)$ is the $\mathbf{H}(n)$ of the TR-MMA. The initial coefficients of the equalization matrix are set uniformly, i.e., $\mathbf{H}_{\mathrm{M}}(0) = \mathbf{H}_{\mathrm{T}}(0)$, $\mathbf{Sig\_out}_{\mathrm{M1}}(0) = \mathbf{Sig\_out}_{\mathrm{T1}}(0) = \mathbf{H}_{\mathrm{T1}}(1) \cdot \mathbf{Sig\_in}(0)$ and $\mathrm{J}_{\mathrm{M1}}(0) = \mathrm{J}_{\mathrm{T1}}(0)$. Comparing with (14a) and (15b), the gradient of $\mathrm{J}_1(n-1)$ is contained in (15b). Hence, the value of $\mathrm{J}_{\mathrm{T1}}(n-1)$ will decrease faster than the value of $\mathrm{J}_{\mathrm{M1}}(n-1)$ in the process of gradient descent, i.e., the value of $\mathrm{J}_{\mathrm{T1}}(n-1) - \mathrm{J}_{\mathrm{T1}}(n)$ will be larger than $\mathrm{J}_{\mathrm{M1}}(n-1) - \mathrm{J}_{\mathrm{M1}}(n)$. Combined $\mathrm{J}_{\mathrm{M1}}(0) = \mathrm{J}_{\mathrm{T1}}(0)$ with $\mathrm{J}_{\mathrm{T1}}(n-1) - \mathrm{J}_{\mathrm{T1}}(n) > \mathrm{J}_{\mathrm{M1}}(n-1) - \mathrm{J}_{\mathrm{M1}}(n)$, the following result is obtained: $\mathrm{J}_{\mathrm{T1}}(n) < \mathrm{J}_{\mathrm{M1}}(n)$, $(n \geq 1)$. For every $\mathbf{Sig\_in}(n-1)$, the equalization effect of $\mathbf{H}_{\mathrm{T}}(n) >$ the equalization effect of $\mathbf{H}_{\mathrm{M}}(n)$, i.e, $\mathbf{H}_{\mathrm{T}}(n)$ is much closer to $\mathbf{H}_{\mathrm{M}}(n+k_{\min}-1)$ than $\mathbf{H}_{\mathrm{M}}(n)$. Hence, for every $\mathbf{Sig\_in}(n-1)$, the equalization effect of $\mathbf{H}_{\mathrm{M}}(n+k_{\min}-1) >$ the equalization effect of $\mathbf{H}_{\mathrm{T}}(n) >$ the equalization effect of $\mathbf{H}_{\mathrm{M}}(n)$. Based on results of Figure 5, we know that for every $\mathbf{Sig\_in}(n)$, the equalization effect of $\mathbf{H}_{\mathrm{M}}(n+k_{\min}) >$ the equalization

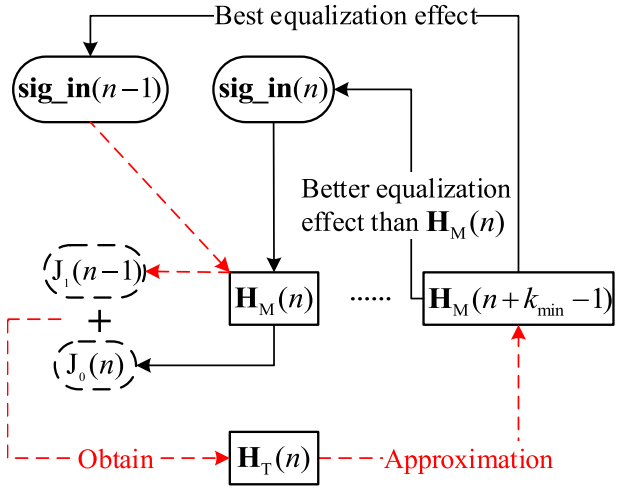

FIGURE 7. Schematic diagram of TR-MMA.

effect of $\mathbf{H}_{\mathrm{M}}(n+k_{\min}-1) > \ldots >$ the equalization effect of $\mathbf{H}_{\mathrm{M}}(n)$. Hence, a new result is drived: for every $\mathbf{Sig\_in}(n)$, the equalization effect of $\mathbf{H}_{\mathrm{M}}(n+k_{\min}) >$ the equalization effect of $\mathbf{H}_{\mathrm{M}}(n+k_{\min}-1) >$ the equalization effect of $\mathbf{H}_{\mathrm{T}}(n) >$ the equalization effect of $\mathbf{H}_{\mathrm{M}}(n)$. It can be seen that the new error can improve the equalization effect of $\mathbf{H}_{\mathrm{M}}(n)$ by adding $\mathrm{J}_1(n-1)$ into the cost function (13a).

The principle of TR-MMA can be summarized as Figure 7. By adding $\mathrm{J}_1(n-1)$ into the cost function (13a), $\mathbf{H}_{\mathrm{T}}(n)$ is much closer to $\mathbf{H}_{\mathrm{M}}(n+k_{\min}-1)$ than $\mathbf{H}_{\mathrm{M}}(n)$ at every time n. As a consequence, for every $\mathbf{Sig\_in}(n)$, $\mathbf{H}_{\mathrm{T}}(n)$ has a better equalization effect than $\mathbf{H}_{\mathrm{M}}(n)$. But the new error term cannot eliminate the hysteresis effect of the equalization matrix. Hence, adding $\mathrm{J}_2(n-2)$ into the cost function $\mathrm{J}_{new}(n)$ can obtain the new cost function $\mathrm{J}_{new2}(n)$ and the new equalization matrix $\mathbf{H}_{\mathrm{T2}}(n)$. For $\mathbf{Sig\_in}(n)$, the equalization effect of $\mathbf{H}_{\mathrm{T2}}(n) >$ the equalization effect of $\mathbf{H}_{\mathrm{T}}(n)$. .... Adding $\mathrm{J}_{k_{\min}}(n-k_{\min})$ into the cost function $\mathrm{J}_{newk_{\min}-1}(n)$ can obtain the new cost function $\mathrm{J}_{newk_{\min}}(n)$ and the new equalization matrix $\mathbf{H}_{\mathrm{T}k_{\min}}(n)$. For $\mathbf{Sig\_in}(n)$, the equalization effect of $\mathbf{H}_{\mathrm{T}k_{\min}}(n) >$ the equalization effect of $\mathbf{H}_{\mathrm{T}k_{\min}-1}(n)$.

In this paper, the number of error terms added into (13a) is written as t, i.e., when $t=1$, $\mathrm{J}_1(n-1)$ is added into (13a), when $t=2$, $\mathrm{J}_1(n-1)$ and $\mathrm{J}_2(n-2)$ are added into (13a) and so on. $\mathrm{J}_k(n-k)$, $(k=1,\ldots,t, 1\le t\le k_{\min})$, is referred to as the time reverse error with tracing back to time $n-k$, which can be added into the cost function (12a). TR-MMA with tracing back to time $n-t$ is referred to as TR-MMA(t) and the cost function $\mathrm{J}_{newt}(n)$ of TR-MMA(t) is given as

$$\mathrm{J}_{newt}(n)=\sum_{k=0}^{t}\beta_k\mathrm{J}_k(n-k), \tag{16a}$$

$$\mathrm{J}_k(n-k)=\mathrm{J}_{k\mathrm{X}}(n-k)+\mathrm{J}_{k\mathrm{Y}}(n-k), \tag{16b}$$

$$\mathrm{J}_{k\mathrm{X}}(n-k)=\mathrm{D}_{k\mathrm{X}}(n-k)\left[\mathrm{q}_k(n-k)^2+\mathrm{p}_k(n-k)^2\right] \tag{16c}$$

$$\mathrm{J}_{k\mathrm{Y}}(n-k)=\mathrm{D}_{k\mathrm{Y}}(n-k)\left[\mathrm{z}_k(n-k)^2+\mathrm{m}_k(n-k)^2\right] \tag{16d}$$

$$\mathrm{q}_k(n-k)=\mathrm{Xout}_{k\mathrm{r}}(n-k)^2-\mathrm{Xideal}_{k\mathrm{r}}(n-k)^2, \tag{16e}$$

$$\mathrm{p}_k(n-k)=\mathrm{Xout}_{k\mathrm{i}}(n-k)^2-\mathrm{Xideal}_{k\mathrm{i}}(n-k)^2, \tag{16f}$$

$$\mathrm{z}_k(n-k)=\mathrm{Yout}_{k\mathrm{r}}(n-k)^2-\mathrm{Yideal}_{k\mathrm{r}}(n-k)^2, \tag{16g}$$

$$\mathrm{m}_k(n-k)=\mathrm{Yout}_{k\mathrm{i}}(n-k)^2-\mathrm{Yideal}_{k\mathrm{i}}(n-k)^2, \tag{16h}$$

$$\begin{aligned}&\mathbf{Sig\_out}_k(n-k)\\&=\begin{bmatrix}\mathrm{Xout}_k(n-k)\\ \mathrm{Yout}_k(n-k)\end{bmatrix}\\&=\mathbf{H}(n)\cdot\mathbf{Sig\_in}(n-k),\end{aligned} \tag{16i}$$

where β_k, $(k=0,1,\ldots,t)$ denotes the weight of each error term, $\mathrm{Xout}_k(n)$ denotes the X-Pol output signal of $\mathbf{Sig\_out}_k(n-k)$, $\mathrm{Yout}_k(n)$ denotes the Y-Pol output signal of $\mathbf{Sig\_out}_k(n-k)$, $\mathrm{J}_{k\mathrm{X}}(n)$ denotes the error of $\mathrm{Xout}_k(n)$, $\mathrm{J}_{k\mathrm{Y}}(n)$ denotes the error of $\mathrm{Yout}_k(n)$, $\mathrm{D}_{k\mathrm{X}}(n-k)$ denotes the probability weight corresponding to the $\mathrm{Xout}_k(n)$, $\mathrm{D}_{k\mathrm{Y}}(n-k)$ denotes the probability weight corresponding to the $\mathrm{Yout}_k(n)$, $\mathrm{Xout}_{k\mathrm{r}}(n)$ and $\mathrm{Xout}_{k\mathrm{i}}(n)$ denote the real and imaginary parts of $\mathrm{Xout}_k(n)$, $\mathrm{Yout}_{k\mathrm{r}}(n)$ and $\mathrm{Yout}_{k\mathrm{i}}(n)$ denote the real and imaginary parts of $\mathrm{Yout}_k(n)$, $\mathrm{Xideal}_{k\mathrm{r}}(n)$ and $\mathrm{Xideal}_{k\mathrm{i}}(n)$ denote the real and imaginary parts of the ideal output of the X-Pol signal of $\mathbf{Sig\_out}_k(n-k)$, $\mathrm{Yideal}_{k\mathrm{r}}(n)$ and $\mathrm{Yideal}_{k\mathrm{i}}(n)$ denote the real and imaginary parts of the ideal output of the Y-Pol signal of $\mathbf{Sig\_out}_k(n-k)$.

The new equalization matrix coefficients update formula is given as

$$\begin{bmatrix}\gamma_s(n+1)\\ \epsilon_s(n+1)\\ \sigma_s(n+1)\end{bmatrix}=\begin{bmatrix}\gamma_s(n)\\ \epsilon_s(n)\\ \sigma_s(n)\end{bmatrix}+\begin{bmatrix}\mu_4\dfrac{\partial\mathrm{J}_{newt}(n)}{\partial\gamma_s(n)}\\ \mu_5\dfrac{\partial\mathrm{J}_{newt}(n)}{\partial\epsilon_s(n)}\\ \mu_6\dfrac{\partial\mathrm{J}_{newt}(n)}{\partial\sigma_s(n)}\end{bmatrix}, \tag{17a}$$

$$\begin{bmatrix}\dfrac{\partial\mathrm{J}_{k\mathrm{X}}(n-k)}{\partial\gamma_s(n)}\\ \dfrac{\partial\mathrm{J}_{k\mathrm{X}}(n-k)}{\partial\epsilon_s(n)}\\ \dfrac{\partial\mathrm{J}_{k\mathrm{X}}(n-k)}{\partial\sigma_s(n)}\end{bmatrix}=\mathbf{V}_{k\mathrm{X}}(n-k)+\mathbf{T}_{k\mathrm{X}}(n-k), \tag{17b}$$

$$\mathbf{V}_{k\mathrm{X}}(n-k)=\begin{bmatrix}\mathrm{Q}_k(n-k)\mathrm{Re}\left\{\mathrm{W}_k(n-k)\right\}\\ \mathrm{Q}_k(n-k)\mathrm{Im}\left\{\mathrm{L}_k(n-k)\right\}cos\gamma_s(n)\\ \mathrm{Q}_k(n-k)\mathrm{Im}\left\{-\mathrm{K}_k(n-k)\right\}sin\gamma_s(n)\end{bmatrix}, \tag{17c}$$

$$\mathbf{T}_{k\mathrm{X}}(n-k)=\begin{bmatrix}\mathrm{P}_k(n-k)\mathrm{Im}\left\{\mathrm{W}_k(n-k)\right\}\\ \mathrm{P}_k(n-k)\mathrm{Re}\left\{-\mathrm{L}_k(n-k)\right\}cos\gamma_s(n)\\ \mathrm{P}_k(n-k)\mathrm{Re}\left\{\mathrm{K}_k(n-k)\right\}sin\gamma_s(n)\end{bmatrix}, \tag{17d}$$

$$\begin{bmatrix}\dfrac{\partial\mathrm{J}_{k\mathrm{Y}}(n-k)}{\partial\gamma_s(n)}\\ \dfrac{\partial\mathrm{J}_{k\mathrm{Y}}(n-k)}{\partial\epsilon_s(n)}\\ \dfrac{\partial\mathrm{J}_{k\mathrm{Y}}(n-k)}{\partial\sigma_s(n)}\end{bmatrix}=\mathbf{V}_{k\mathrm{Y}}(n-k)+\mathbf{T}_{k\mathrm{Y}}(n-k), \tag{17e}$$

$$\mathbf{V}_{k\mathrm{Y}}(n-k)=\begin{bmatrix}\mathrm{Z}_k(n-k)\mathrm{Re}\left\{\mathrm{W}_k(n-k)\right\}\\ \mathrm{Z}_k(n-k)\mathrm{Im}\left\{\mathrm{L}_k(n-k)\right\}cos\gamma_s(n)\\ \mathrm{Z}_k(n-k)\mathrm{Im}\left\{-\mathrm{K}_k(n-k)\right\}sin\gamma_s(n)\end{bmatrix}, \tag{17f}$$

$$\mathbf{T}_{k\mathrm{Y}}(n-k) = \begin{bmatrix} \mathrm{M}_k(n-k)\mathrm{Im}\{\mathrm{W}_k(n-k)\} \\ \mathrm{M}_k(n-k)\mathrm{Re}\{-\mathrm{L}_k(n-k)\}\, cos\gamma_s(n) \\ \mathrm{M}_k(n-k)\mathrm{Re}\{\mathrm{K}_k(n-k)\}\, sin\gamma_s(n) \end{bmatrix}, \tag{17g}$$

$$\mathrm{L}_k(n-k) = e^{-\mathrm{j}\epsilon_s(n)}\mathrm{Xin}(n-k), \tag{17h}$$

$$\mathrm{K}_k(n-k) = -e^{-\mathrm{j}\sigma_s(n)}\mathrm{Yin}(n-k), \tag{17i}$$

$$\mathrm{W}_k(n-k) = -\mathrm{L}_k(n-k)sin\gamma_s(n) + \mathrm{K}_k(n-k)cos\gamma_s(n), \tag{17j}$$

$$\mathrm{Q}_k(n-k) = \mathrm{Xout}_{kr}(n-k)\mathrm{q}_k(n-k), \tag{17k}$$

$$\mathrm{P}_k(n-k) = \mathrm{Xout}_{ki}(n-k)\mathrm{p}_k(n-k), \tag{17l}$$

$$\mathrm{Z}_k(n-k) = \mathrm{Yout}_{kr}(n-k)\mathrm{z}_k(n-k), \tag{17m}$$

$$\mathrm{M}_k(n-k) = \mathrm{Yout}_{ki}(n-k)\mathrm{m}_k(n-k). \tag{17n}$$

B. ALGORITHM DESIGN

To reduce the BER of MMA, a new TR-MMA has been designed for coherent optical PDM systems by adding the time reverse errors into the cost function. The algorithm is summarized as follows:

Algorithm 1 TR-MMA(t)

Input: Input signal matrix **Sig_in**(n); Initial value of the equalization matrix **H**(1); Number of symbols N; Symbol transmission rate f_s; Speed of RSOP ω; Value of t; Weight β_k and step size μ_4, μ_5 and μ_6

Output: Output signal matrix $\mathbf{Sig\_out}_0(n)$.

1 Set input parameters and initialize the equalization matrix **H**(1) randomly
2 Generate k groups of the input signal according to (6) and set them as **Sig_in**(0), $\mathbf{Sig\_in}(-1), \ldots, \mathbf{Sig\_in}(1-t)$.
3 **for** $n = 1 : N$ **do**
4 Receive **Sig_in**(n)
5 Calculate $\mathbf{Sig\_in}_0(n)$, $\mathbf{Sig\_in}_1(n-1), \ldots, \mathbf{Sig\_in}_t(n-t)$ according to (16i)
6 Calculate $\begin{bmatrix} \gamma_s(n+1) \\ \epsilon_s(n+1) \\ \sigma_s(n+1) \end{bmatrix}$ according to (17a)
7 Calculate **H**$(n+1)$ according to $\begin{bmatrix} \gamma_s(n+1) \\ \epsilon_s(n+1) \\ \sigma_s(n+1) \end{bmatrix}$
8 **end**

IV. SIMULATION RESULTS

In this section, we analyze the BER and the mean square error (MSE) of the TR-MMA and the MMA in 16 QAM coherent optical PDM systems. In Figure 5, $k_{\min}$ is 19 for two times, 20 for one time and 22 for one time. Hence, without loss of generality, we set $t = 1, 5$ for simulation. SNR is 20dB, N is 2^{18}, f_s is 28 Gbaud/s, μ_1, μ_2 and μ_3 are $1.4 \times 5 \times 10^{-4}$, $1.4 \times 1.6 \times 10^{-6}$ and $1.4 \times 1.5 \times 10^{-5}$, respectively, μ_4, μ_5 and μ_6 are 5×10^{-4}, 1.6×10^{-6} and 1.5×10^{-5}, respectively, f_c is 1GHz, v is 1MHz and β_k, $(k = 1, 2, \ldots, 5)$ are 1, 0.8, 0.6, 0.4, 0.2, 0.1, respectively.

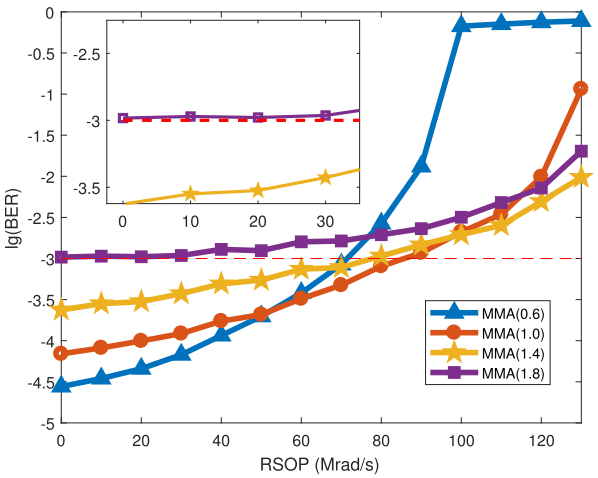

FIGURE 8. lg(BER) of the MMA with different μ_1, μ_2 and μ_3.

The BER and MSE are the average value of 50 cycles of simulations.

The cost function of the TR-MMA (16a) is different from the cost function of the MMA (13a), so the optimal step sizes of the TR-MMA and MMA are different. To illustrate the improvement of TR-MMA in BER and MSE compared to MMA, the step sizes of MMA μ_1, μ_2 and μ_3 need to be tuned. Figure 8 shows the lg(BER) of the MMA with different μ_1, μ_2 and μ_3. In Figure 8, MMA(0.6) denotes the MMA with $\mu_1 = 0.6 \times 5 \times 10^{-4}$, $\mu_2 = 0.6 \times 1.6 \times 10^{-6}$ and $\mu_3 = 0.6 \times 1.5 \times 10^{-5}$, MMA(1.0) denotes the MMA with $\mu_1 = 1.0 \times 5 \times 10^{-4}$, $\mu_2 = 1.0 \times 1.6 \times 10^{-6}$ and $\mu_3 = 1.0 \times 1.5 \times 10^{-5}$, MMA(1.4) denotes the MMA with $\mu_1 = 1.4 \times 5 \times 10^{-4}$, $\mu_2 = 1.4 \times 1.6 \times 10^{-6}$ and $\mu_3 = 1.4 \times 1.5 \times 10^{-5}$ and MMA(1.8) denotes the MMA with $\mu_1 = 1.8 \times 5 \times 10^{-4}$, $\mu_2 = 1.8 \times 1.6 \times 10^{-6}$ and $\mu_3 = 1.8 \times 1.5 \times 10^{-5}$. The lg(BER) of the MMA(0.6), MMA(1.0), MMA(1.4) and MMA(1.8) increase with the increase of RSOP. Without loss of generality, -3 is configured as the upper bound of the lg(BER) for 16 QAM coherent optical PDM systems [37]. Hence, the MMA(1.8) is not acceptable. Furthermore, when the RSOP is changed from 0 Mrad/s to 130 Mrad/s, the average BER of the MMA(1.4) is 99.13% lower than the average BER of the MMA(0.6) and the average BER of the MMA(1.4) is 81.04% lower than the average BER of the MMA(1.0). The reduction rate of the average BER is calculated by

$$\eta_1 = 1 - \frac{\sum_{k=0}^{13} \mathrm{BER}_2(k)}{\sum_{k=0}^{13} \mathrm{BER}_1(k)}, \tag{18}$$

where $\mathrm{BER}_2(k)$ denotes the BER value of the MMA(1.4) when RSOP $= 10k$ Mrad/s and $\mathrm{BER}_2(k)$ denotes the BER value of the MMA(0.6) or MMA(1.0) when RSOP $= 10k$ Mrad/s. Hence, the step sizes of the MMA μ_1, μ_2 and μ_3 are $1.4 \times 5 \times 10^{-4}$, $1.4 \times 1.6 \times 10^{-6}$ and $1.4 \times 1.5 \times 10^{-5}$, respectively.

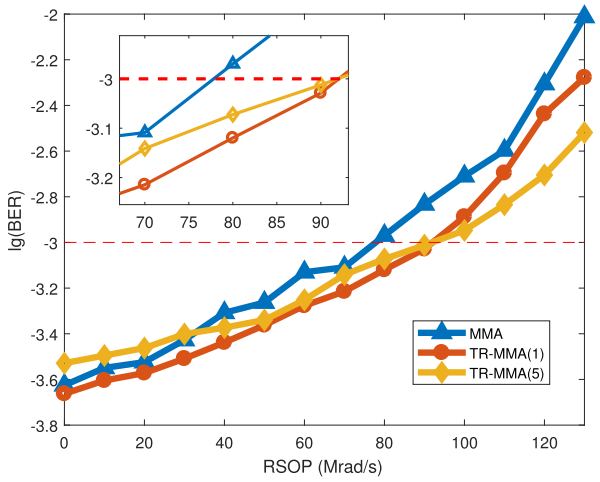

FIGURE 9. lg(BER) of the MMA, TR-MMA(1) and TR-MMA(5).

Figure 9 shows the lg(BER) of the MMA, TR-MMA(1) and TR-MMA(5). The lg(BER) of the MMA, TR-MMA(1) and TR-MMA(5) increase with the increase of RSOP. When the RSOP is fixed, the lg(BER) of the TR-MMA(1) is lower than the lg(BER) of MMA. When the RSOP is fixed and RSOP $>$ 90 Mrad/s, the lg(BER) of the TR-MMA(5) is lower than the lg(BER) of the TR-MMA(1). The average BER of the TR-MMA(1) is 33.47% lower than the average BER of the MMA when the RSOP is changed from 0 Mrad/s to 130 Mrad/s. The average BER of the TR-MMA(5) is 23.54% lower than the average BER of the TR-MMA(1) when the RSOP is changed from 0 Mrad/s to 130 Mrad/s. The reduction rate of the average BER is calculated by

$$\eta_2 = 1 - \frac{\sum_{k=0}^{13} \mathrm{BER}_{\mathrm{TR-MMA(1)}}(k)}{\sum_{k=0}^{13} \mathrm{BER}_{\mathrm{MMA}}(k)}, \tag{19}$$

where $\mathrm{BER}_{\mathrm{TR-MMA(1)}}(k)$ denotes the BER value of the TR-MMA(1) when RSOP $= 10k$ Mrad/s and $\mathrm{BER}_{\mathrm{MMA}}(k)$ denotes the BER value of the MMA when RSOP $= 10k$ Mrad/s. When the lg(BER) is less than the upper bound, i.e., -3, the corresponding maximum value of RSOP is the RSOP tolerance of the equalization algorithm. Results of Figure 9 indicate that the RSOP tolerance of the MMA is 70 Mrad/s and the RSOP tolerances of the TR-MMA(1) and TR-MMA(5) are 90 Mrad/s. Compared with the RSOP tolerance of the MMA, the RSOP tolerances of the TR-MMA(1) and TR-MMA(5) are increased by 28.57%.

Figure 10 shows the MSE of the MMA and TR-MMA(1) with RSOP $=$ 130 Mrad/s. MSE is one of key indexes for coherent optical PDM systems. In this paper, the MSE is calculated by

$$\mathrm{MSE}(n) = \frac{1}{2n}\sum_{i=1}^{n} \mathrm{S}(i), \tag{20a}$$

$$\mathrm{S}(i) = \left[|\mathrm{X}(i) - \mathrm{Xout}(i)|^2 + |\mathrm{Y}(i) - \mathrm{Yout}(i)|^2\right], \tag{20b}$$

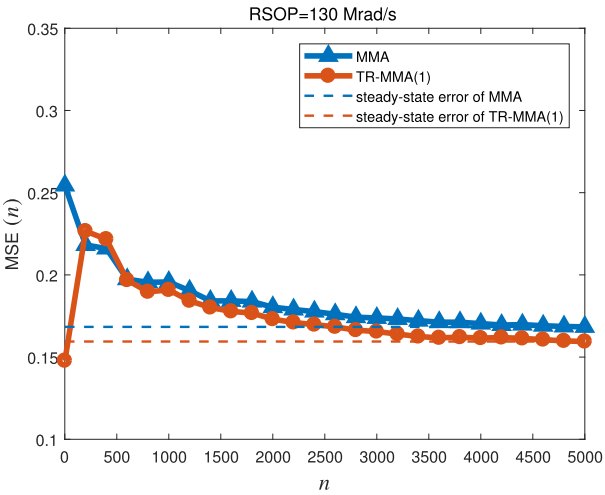

FIGURE 10. MSE of the MMA and TR-MMA(1).

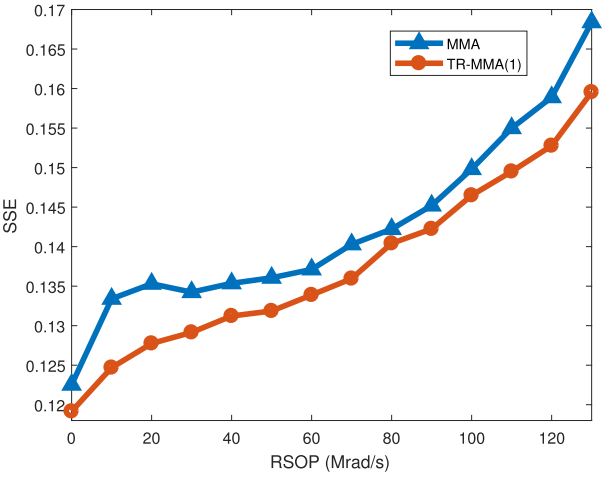

FIGURE 11. SSE of the MMA and TR-MMA(1).

where i is the i-th time and $|\cdot|$ is the modulo operation. The SSE is the convergent value of MSE. Based on results of Figure 10, the MSE of the MMA and TR-MMA(1) decrease with the increase of time n. Results of Figure 10 indicate that the SSE of the MMA and TR-MMA(1) are 0.1684 and 0.1595, respectively. Figure 11 shows the SSE of the MMA and TR-MMA(1) with different RSOPs. Based on results of Figure 11, the SSE of the MMA and TR-MMA(1) increase with the increase of RSOP. When the RSOP is fixed, the SSE of TR-MMA(1) is lower than the SSE of MMA. Compared with the average SSE of the MMA, the average SSE of the TR-MMA(1) is reduced by 4.08% when the RSOP is changed from 0 Mrad/s to 130 Mrad/s. The reduction rate of the average SSE is calculated by

$$\eta_3 = 1 - \frac{\sum_{k=0}^{13} \mathrm{SSE}_{\mathrm{TR-MMA(1)}}(k)}{\sum_{k=0}^{13} \mathrm{SSE}_{\mathrm{MMA}}(k)}, \tag{21}$$

where $\mathrm{SSE}_{\mathrm{TR-MMA(1)}}(k)$ denotes the SSE value of the TR-MMA(1) when RSOP $= 10k$ Mrad/s and $\mathrm{SSE}_{\mathrm{MMA}}(k)$ denotes the SSE value of the MMA when RSOP $= 10k$ Mrad/s.

V. CONCLUSION

In this paper, the hysteresis effect of the equalization matrix is first investigated for coherent optical PDM communication systems. Moreover, the hysteresis effect of the equalization matrix is proposed as a time reverse error term to correct the equalization matrix coefficient and fast the convergence speed of output signal errors. Furthermore, a new equalization algorithm based on time reverse error is developed to reduce the BER of coherent optical PDM communication systems. Compared with the MMA, simulation results show that the average BER and SSE of the TR-MMA(1) is reduced by 33.47% and 4.08%, respectively. Moreover, the RSOP tolerance of the TR-MMA(1) is increased by 28.57% compared with the MMA.

REFERENCES

[1] X. Ge, B. Yang, J. Ye, G. Mao, C.-X. Wang, and T. Han, "Spatial spectrum and energy efficiency of random cellular networks," *IEEE Trans. Commun.*, vol. 63, no. 3, pp. 1019–1030, Mar. 2015.
[2] A. Nainggolan, H.-M. Hsia, Y.-H. Chen, C.-Y. Li, W.-S. Tsai, and H.-H. Lu, "A PDM-based 168 Gb/s VSB-PAM8 fiber-FSO integration," in *Proc. 14th Pacific Rim Conf. Lasers Electro-Opt. (CLEOPR)*, 2020, Paper C3F_1, pp. 1–2.
[3] X. Li, M. O'Sullivan, Z. Xing, M. Alam, T. Hoang, M. Xiang, M. Zhu, J. Zhang, E. Elfiky, and D. Plant, "Asymmetric direct detection of orthogonal offset carriers assisted polarization multiplexed single-sideband signals," *Opt Exp.*, vol. 28, pp. 3226–3236, Oct. 2020.
[4] D. Kakati and R. K. Sonkar, "A 2×320 gbps hybrid PDM-MDM-OFDM system for high-speed terrestrial FSO communication," in *Proc. 14th Pacific Rim Conf. Lasers Electro-Opt. (CLEOPR)*, 2020, pp. 1–2, Paper C5F_3.
[5] P. Vijarnstit, R. Maneekut, and P. Kaewplung, "A flexible fiber access network using superchannel coherent optical orthogonal frequency division multiplexing," in *Proc. 17th Int. Conf. Adv. Commun. Technol. (ICACT)*, Jul. 2015, pp. 319–322.
[6] J. Liu, B. Liu, X. Zeng, J. Lu, and H. Shi, "Polarization de-multiplexing algorithm based on twice real-valued FastICA," in *Proc. Optoelectron. Global Conf. (OGC)*, Shenzhen, China, Aug. 2015, pp. 1–4.
[7] C. Wang, X. Li, M. Zhao, K. Wang, J. Zhang, M. Kong, W. Zhou, J. Xiao, and J. Yu, "Delivery of 138.88 Gpbs signal in a RoF network with real-time processing based on heterodyne detection," in *Proc. Opt. Fiber Commun. Conf. (OFC)*, 2020, pp. 1–3, Paper W2A.42.
[8] D. Charlton, S. Clarke, D. Doucet, M. O'Sullivan, D. L. Peterson, D. Wilson, G. Wellbrock, and M. Bélanger, "Field measurements of SOP transients in OPGW, with time and location correlation to lightning strikes," *Opt. Exp.*, vol. 25, no. 9, pp. 9689–9696, 2017.
[9] P. M. Krummrich and K. Kotten, "Extremely fast (microsecond timescale) polarization changes in high speed long haul WDM transmission systems," in *Proc. Opt. Fiber Commun. Conf.*, 2004, pp. 1–3, Paper FI3.
[10] P. M. Krummrich, D. Ronnenberg, W. Schairer, D. Wienold, F. Jenau, and M. Herrmann, "Demanding response time requirements on coherent receivers due to fast polarization rotations caused by lightning events," *Opt. Exp.*, vol. 24, no. 11, pp. 12442–12457, 2016.
[11] N. Cui, X. Zhang, Z. Zheng, H. Xu, W. Zhang, X. Tang, L. Xi, Y. Fang, and L. Li, "Two-parameter-SOP and three-parameter-RSOP fiber channels: Problem and solution for polarization demultiplexing using Stokes space," *Opt Exp.*, vol. 26, pp. 21170–21183, Oct. 2018.
[12] S. Abrar, "Sliced multi-modulus blind equalization algorithm," *ETRI J.*, vol. 27, no. 3, pp. 257–266, Jun. 2005.
[13] J. G. Proakis and D. G. Manolakis, *Introduction to Digital Signal Processing*. Upper Saddle River, NJ, USA: Prentice-Hall, 1988.
[14] D. Godard, "Self-recovering equalization and carrier tracking in two-dimensional data communication systems," *IEEE Trans. Commun.*, vol. 28, no. 11, pp. 1867–1875, Nov. 1980.
[15] S. J. Savory, G. Gavioli, R. I. Killey, and P. Bayvel, "Transmission of 42.8 Gbit/s polarization multiplexed NRZ-QPSK over 6400km of standard fiber with no optical dispersion compensation," in *Proc. Conf. Opt. Fiber Commun. Nat. Fiber Optic Eng. Conf.*, Mar. 2007, pp. 1–3, Paper OTuA1.
[16] Z. Yu, X. Yi, J. Zhang, M. Deng, H. Zhang, and K. Qiu, "Modified constant modulus algorithm with polarization demultiplexing in Stokes space in optical coherent receiver," *J. Lightw. Technol.*, vol. 31, no. 19, pp. 3203–3209, Oct. 13, 2013.
[17] G. Bosco, M. Visintin, P. Poggiolini, and F. Forghieri, "A novel update algorithm in Stokes space for adaptive equalization in coherent receivers," in *Proc. Opt. Fiber Commun. Conf.*, San Francisco, CA, USA, 2014, pp. 1–3.
[18] B. Szafraniec, B. Nebendahl, and T. Marshall, "Polarization demultiplexing in Stokes space," *Opt. Exp.*, vol. 18, no. 17, pp. 17928–17939, 2010.
[19] B. Szafraniec, T. S. Marshall, and B. Nebendahl, "Performance monitoring and measurement techniques for coherent optical systems," *J. Lightw. Technol.*, vol. 31, no. 4, pp. 648–663, Feb. 3, 2013.
[20] S. Ziaie, N. J. Muga, F. P. Guiomar, G. M. Fernandes, R. M. Ferreira, A. Shahpari, A. L. Teixeira, and A. N. Pinto, "Experimental assessment of the adaptive Stokes space-based polarization demultiplexing for optical metro and access networks," *J. Lightw. Technol.*, vol. 33, no. 23, pp. 4968–4974, Dec. 1, 2015.
[21] R. Borkowski, D. Zibar, A. Caballero, V. Arlunno, and I. T. Monroy, "Stokes space-based optical modulation format recognition for digital coherent receivers," *IEEE Photon. Technol. Lett.*, vol. 25, no. 21, pp. 2129–2132, Nov. 2013.
[22] N. J. Muga and A. N. Pinto, "Digital PDL compensation in 3D Stokes space," *J. Lightw. Technol.*, vol. 31, no. 13, pp. 2122–2130, Jul. 2013.
[23] N. J. Muga and A. N. Pinto, "Adaptive 3-D Stokes space-based polarization demultiplexing algorithm," *J. Lightw. Technol.*, vol. 32, no. 19, pp. 3290–3298, Oct. 1, 2014.
[24] D. Gesbert, P. Duhame, and S. Mayrargue, "On-line blind multichannel equalization based on mutually referenced filters," *IEEE Trans. Signal Process.*, vol. 45, no. 9, pp. 2307–2317, Sep. 1997.
[25] J. Yang, J.-J. Werner, and G. A. Dumont, "The multimodulus blind equalization and its generalized algorithms," *IEEE J. Sel. Areas Commun.*, vol. 20, no. 5, pp. 997–1015, Jun. 2002.
[26] D. Zhao, L. Xi, X. Tang, W. Zhang, Y. Qiao, and X. Zhang, "Digital pilot aided carrier frequency offset estimation for coherent optical transmission systems," *Opt Exp.*, vol. 23, pp. 24822–24832, Dec. 2015.
[27] Y. Chen, Q. Sui, Z. Li, Z. Liang, and W. Liu, "Joint CD and PMD monitoring based on a pair of low-bandwidth coherent receivers," *Opt Exp.*, vol. 24, pp. 26756–26765, Oct. 2016.
[28] J. Wang, Z. Chen, S. Fu, Y. Wang, and Y. Qin, "Fast and blind chromatic dispersion estimation with one sample per symbol," *Opt Exp.*, vol. 29, pp. 7504–7513, May 2021.
[29] R. A. Soriano, F. N. Hauske, N. G. Gonzalez, Z. Zhang, Y. Ye, and I. T. Monroy, "Chromatic dispersion estimation in digital coherent receivers," *J. Lightw. Technol.*, vol. 29, no. 11, pp. 1627–1637, Jun. 18, 2011.
[30] S. A. Sheikh and P. Fan, "A new multimodulus blind equalizer for dense QAM constellations," in *Proc. IET Int. Conf. Wireless Mobile Multimedia Netw. Proc. (ICWMMN)*, hangzhou, China, 2006, pp. 1–4.
[31] L. Li, Y. Feng, W. Zhang, N. Cui, H. Xu, X. Tang, L. Xi, and X. Zhang, "A joint recovery scheme for carrier frequency offset and carrier phase noise using extended Kalman filter," *Opt. Fiber Technol.*, vol. 36, pp. 438–446, Jul. 2017.
[32] J. Liu and G.-K. Chang, "Enhancement of the laser phase noise tolerance for star 16-QAM optical coherent systems," in *Proc. Opt. Transmiss. Syst., Subsystems, Technol.*, 2011.
[33] M. P. Paskov, *Algorithms and Subsystems for Next Generation Optical Networks*. London, U.K.: Univ. College London, 2015.
[34] N. Mehrdad, M. Derakhtian, and M. Masnadi-Shirazi, "Steady-state performance analysis of a generalised multimodulus adaptive blind equalisation based on the pseudo Newton algorithm," *IET Signal Process.*, vol. 6, no. 1, pp. 14–26, 2012.
[35] S. S. Haykin, *Adaptive Filter Theory*. London, U.K.: Pearson, 2008.
[36] D. Lavery, M. Paskov, R. Maher, S. J. Savory, and P. Bayvel, "Modified radius directed equaliser for high order QAM," in *Proc. Eur. Conf. Opt. Commun. (ECOC)*, Valencia, Spain, Sep. 2015, pp. 1–3.
[37] M. I. Khalil, M. M. H. Adib, A. M. Chowdhury, M. S. Faruk, and G.-K. Chang, "A novel algorithm for blind joint equalization and carrier phase estimation in 16-QAM coherent optical communication," in *Proc. 7th Int. Conf. Electr. Comput. Eng.*, Dhaka, Bangladesh, Dec. 2012, pp. 563–566.

JUNXIONG ZHANG received the B.E. degree in electromagnetic field and wireless technology from the Huazhong University of Science and Technology (HUST), Wuhan, China, in 2019, where he is currently pursuing the M.E. degree. His research interest includes coherent optical polarization division multiplexing (PDM) technology.

WEIMIN WU received the B.E. degree in computer software from Xidian University, Xi'an, China, in 1992, the M.E. degree in computer application from Sichuan University, Chengdu, China, in 1995, and the Ph.D. degree in communications and information systems from the Huazhong University of Science and Technology, Wuhan, China, in 2007. He is currently an Associate Professor with the School of Electronic Information and Communications, Huazhong University of Science and Technology. His current research interests include the areas of Internet streaming, broadband wireless communications, and networking.

XIAOHU GE (Senior Member, IEEE) received the Ph.D. degree in communication and information engineering from the Huazhong University of Science and Technology (HUST), Wuhan, China, in 2003. He has been working with HUST, since November 2005. Prior to that, he was a Researcher with Ajou University, Suwon, South Korea, and the Politecnico di Torino, Turin, Italy, from January 2004 to October 2005. He was a Visiting Researcher with Heriot-Watt University, Edinburgh, U.K., from June 2010 to August 2010. He is currently a Full Professor with the School of Electronic Information and Communications, HUST. He is also an Adjunct Professor with the Faculty of Engineering and Information Technology, University of Technology Sydney (UTS), Sydney, NSW, Australia. He has authored over 100 papers in refereed journals and conference proceedings and has been granted over 15 Chinese patents. He is leading several projects funded by NSFC, MOST of China, and industries. He is taking part in several international joint projects, such as the EU FP7-PEOPLE-IRSES: project acronym WiNDOW and project acronym CROWN. His research interests include mobile communications, traffic modeling in wireless networks, green communications, and interference modeling in wireless communications. He is a Senior Member of the China Institute of Communications and a member of the National Natural Science Foundation of China and the Chinese Ministry of Science and Technology Peer-Review College. He was a recipient of the best paper awards from the IEEE GLOBECOM 2010. He has been actively involved in organizing more than ten international conferences, since 2005. He has served as the General Chair for the 2015 IEEE International Conference on Green Computing and Communications (IEEE GreenCom). He serves as an Associate Editor for IEEE Access, *Wireless Communications and Mobile Computing* journal (Wiley), and the *International Journal of Communication Systems* (Wiley). Moreover, he served as a Guest Editor for the *IEEE Communications Magazine* Special Issue on 5G Wireless Communication Systems.